Available online at www.sciencedirect.com
SCIENCE DIRECT
International Journal of Heat and Fluid Flow 26 (2005) 865–872
International Journal of HEAT AND FLUID FLOW
www.elsevier.com/locate/ijhff

A bench top experimental model of bubble transport in multiple arteriole bifurcations

Brijesh Eshpuniyani, J. Brian Fowlkes, Joseph L. Bull *

The University of Michigan, Ann Arbor, MI 48109, USA

Available online 7 November 2005

Abstract

Motivated by a novel gas embolotherapy technique, a bench top vascular bifurcation model is used to investigate the splitting of long bubbles in a series of liquid-filled bifurcations. The developmental gas embolotherapy technique aims to treat cancer by infarcting tumors with gas emboli that are formed by selective acoustic vaporization of ~6 μm, intravascular, perfluorcarbon droplets. The resulting gas bubbles are large enough to extend through several vessel bifurcations. The current bench top experiments examine the effects of gravity and flow on bubble transport through multiple bifurcations. The effect of gravity is varied by changing the roll angle of the bifurcating network about its parent tube. Splitting at each bifurcation is nearly even when the roll angle is zero. It is demonstrated that bubbles can either stick at one of the second bifurcations or in the second generation daughter tubes, even though the flow rate in the parent tube is constant. The findings of this work indicate that both gravity and flow are important in determining the bubble transport, and suggest that a treatment strategy that includes multiple doses may be effective in delivering emboli to vessels not occluded by the initial dose.

Keywords: Gas embolotherapy; Air embolism; Cardiovascular emboli

1. Introduction

A bench top vascular bifurcation model is used to investigate the splitting of long bubbles in a series of liquid-filled bifurcations. These experiments are motivated by a gas embolotherapy technique (Kripfgans et al., 2000, 2002; Bull, 2003; Kripfgans et al., 2004; Ye and Bull, 2004b; Bull, 2005) that we are developing for the potential treatment of cancer by using gas emboli to infarct tumors. Gas embolotherapy is described in more detail elsewhere (Bull, 2005). The gas bubbles originate as perfluorocarbon droplets that are small enough to pass through capillaries and are injected into the bloodstream. Low intensity ultrasound is used to track their motion, and they are vaporized at the desired location for treatment via high intensity ultrasound to produce gas bubbles whose volumes are approximately 125 to 150 times the droplet volume. The liquid droplets are stabilized by an albumin shell, and the acoustic droplet vaporization may occur as a result of disruption of this albumin shell (Kripfgans et al., 2000, 2002, 2004). The resulting gas bubbles are large enough to occlude capillaries and have persistence times on the order of days, indicating their potential to infarct tumors. In other studies, we have computationally investigated the potential of this bubble vaporization to damage or rupture vessels (Ye and Bull, 2004a,b).

Achieving complete tumor necrosis requires infarction of most of the tumor. However, it has been shown that embolotherapy can be successful with partial necrosis (success has been observed with about 78% tumor necrosis for solid emboli) (Di Segni et al., 1997). Understanding the transport and splitting of the gas bubbles, which can be long enough to extend through more than one bifurcation, is necessary in order to design delivery strategies.

In previous studies of bubble transport through a single bifurcation in which one branch of the bifurcation was higher than the other, we have demonstrated that flow and gravity compete to determine the splitting dynamics

* Corresponding author.
E-mail address: joebull@umich.edu (J.L. Bull).

0142-727X/$ - see front matter © 2005 Elsevier Inc. All rights reserved.
doi:10.1016/j.ijheatfluidflow.2005.10.002

of the bubble (Calderon and Bull, 2004; Calderon et al., 2005). For slow enough flows and strong enough gravitational effects, the entire bubble travels into the upper branch of the bifurcation. Below a critical value of the flow rate, the bubble does not split. For stronger flows and/or weaker gravitational effects, the bubble will split and the splitting is more homogeneous at higher flow rates. Motivated by air embolism, previous studies of bubbles in single, straight, inclined tubes have shown that gravity can oppose flow to immobilize bubbles (Cavanagh and Eckmann, 1999, 2002; DeBisschop et al., 2002). Previous researchers have studied scenarios wherein air bubbles stick in the microcirculation (Suzuki and Eckmann, 2003), and have investigated the usefulness of surfactants in dislodging emboli (Eckmann et al., 2001; Branger and Eckmann, 2002; Cavanagh and Eckmann, 2002; Eckmann and Cavanagh, 2003; Eckmann and Diamond, 2004; Suzuki et al., 2004). The single bifurcation experiments (Calderon and Bull, 2004; Calderon et al., 2005) did not consider bubble sticking as the minimum vessel size modeled in that study was still too large to allow for bubble sticking in the flow conditions considered.

The current experiments investigate the behavior of a bubble as it passes through a series of two geometrically symmetric bifurcations. The bubbles in gas embolotherapy are long compared to the vessel diameter, and may extend through more than one vessel bifurcation at a time. Few previous investigations have considered the transport of bubbles through bifurcations and have primarily focused on bubbles or droplets that are small compared to the tube diameter (Chang et al., 1981; Manga, 1996). This investigation provides new information about the dynamics of long bubbles in bifurcating vessel networks. Additionally, the tube diameters after the second set of bifurcations are small enough to allow the possibility of bubble sticking.

A range of effective Bond numbers, which depend on gravity and the positioning of the bifurcation, and capillary numbers are investigated. The experiments are designed to match the Reynolds, Bond and capillary numbers to the physiological values for arterioles, and provide guidance in achieving a uniform delivery of bubbles to tumor vasculature. This study investigates the splitting and sticking behavior of bubbles in multiple bifurcations and may also be applicable to air embolism.

2. Experiments

A sketch of the bifurcating network model is shown in Fig. 1. The parent tube (referred to as generation 0 and denoted by the label L0 in Fig. 1) divides into two first generation daughter tubes (labeled L1 and L2 in Fig. 1) at the first bifurcation. These daughter tubes split at the two second generation bifurcations into four second generation daughter tubes (labeled L3, L4, L5, and L6 in Fig. 1). The dimensions in Fig. 1 are in units of centimeters. The diameter of the parent tube is 0.1 cm. Each set of successive generation tubes has a diameter 0.78 times the diameter of the previous generation. The branching angle at both the bifurcations is 78°. These values are chosen to match physiological values for arterioles (Fung, 1997; Calderon et al., 2005).

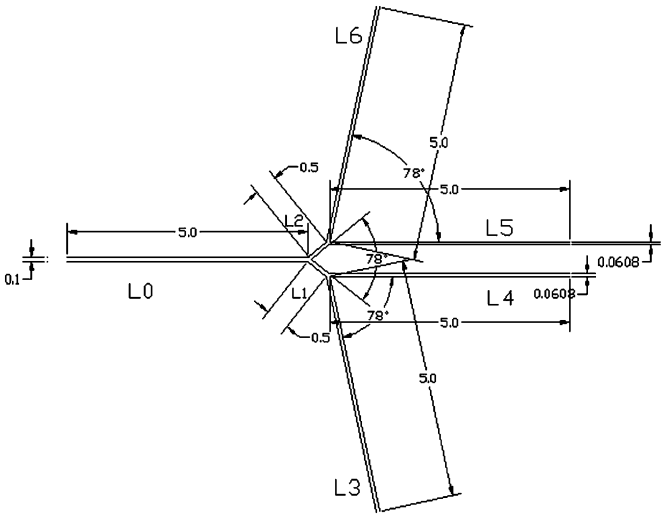

Fig. 1. Sketch of experimental setup (to scale). The parent tube (generation 0, labeled segment L0) bifurcates into first generation daughter tubes (denoted by L1 and L2), each of which further bifurcate into second generation daughter tubes (denoted by L3–L6). The bifurcation angle is 78° at each bifurcation and the diameter of each generation of tubes is 0.78 times the diameter of the previous generation. The geometry was chosen to match typical physiological geometry for arterioles. Dimensions are in centimeters.

The bifurcation model (Fig. 2) was made using 5-inch square, 0.2-inch thick, cast acrylic sheets (McMaster-Carr, Chicago, IL). The circular cross-section of the channels was achieved by machining semicircular channels in two mirror halves, followed by aligning the two halves with locator pins and bolting them together. To accomplish the circular lumen, ball-end mills (Fullerton Tool Co. Sag-

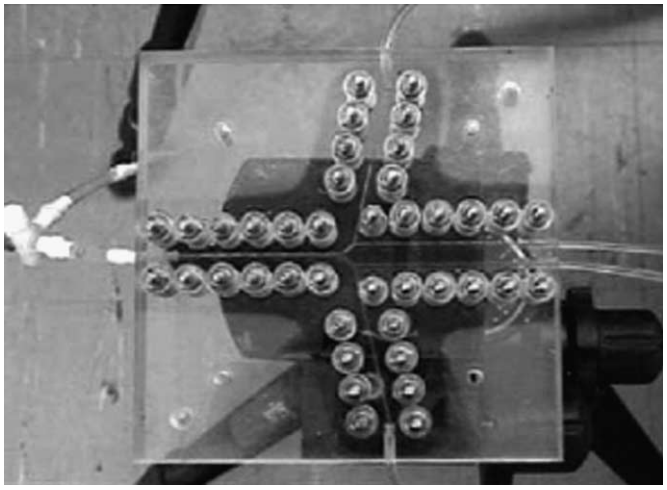

Fig. 2. Experimental bifurcating tube network. Tygon tubing connects the test section to the syringe pump and to the constant pressure reservoirs.

inaw, MI) of 0.04, 0.031 and 0.024 inches diameter were used to machine the channel branches of respective diameters. All machining was performed using a 3-axis mill (Chevalier Machinery Inc., Santa Fe Springs, CA) with programmable CNC (Milltronics Manufacturing, Waconia, MN). Forty through-holes were drilled along the perimeter of the bifurcating channel and in two 5-inch square, 0.35-inch thick, cast acrylic sheets, which were placed above and below the mated channel, and 1-inch long, 6/32 binding screws, flat washers, and nuts (McMaster-Carr, Chicago, IL) are used to bolt the two halves together ensuring a tight seal to avoid any leakage.

The parent tube of the model bifurcation was connected to a syringe pump (PHD 2000 Programmable, Harvard Apparatus Inc., Holliston, MA) and the outlets of the daughter tubes were connected to reservoirs via Tygon tubing. The reservoirs were open to the atmosphere and were allowed to overflow so that each free surface was maintained at a constant elevation. This configuration resulted in constant reservoir pressures that were the same for each reservoir. The experiments were conducted at room temperature. The blood phase was modeled by filtered water and the perfluorocarbon bubble was modeled by an air bubble. The two mirror halves of the bifurcating channel were cleaned thoroughly at regular periods using soap and water.

In each experiment, an air bubble was placed into the parent tube by a microliter syringe inserted through a side port connector in the experimental circuit. The bubble was placed a sufficient distance upstream from the bifurcation so that the bubble and surrounding water reach steady flow far in front of the bifurcation. Flow from the syringe pump into the parent tube of the bifurcation was set to a constant value and the motion of the bubble through the bifurcation was imaged by a CCD camera and recorded on digital video tape (DCR-PC110, Sony, Tokyo, Japan).

These digital videos were then transferred to a computer (Dell PC, Round Rock, TX) and converted to sequenced bitmap images for analysis using Adobe Premier (Adobe Systems Incorporated, San Jose, CA). From image analysis, the length of the bubbles in each of the branches of the two bifurcations was measured. These length measurements are made after the bubble splitting is complete. This includes scenarios where the initial bubble goes through both the bifurcations, with portions of the initial bubble having reached the four second generation daughter tubes, as well as scenarios where a portion of the initial bubble gets stuck at one of the second generation bifurcations and the remaining bubble reaches the second generation daughter tubes. Volume of these bubbles was then computed by multiplying the length with the cross-sectional area of the corresponding branch.

A range of flow rates and roll angles were investigated. While the flow rate is set using the syringe pump that drives the flow, the roll angle is defined as the angle made by the plane of the bifurcation (all tubes are in the same plane) with the horizontal. The roll angle is varied by rotating the bifurcation plane about the axis passing through the parent tube. The flow conditions are set to match different non-dimensional parameter values to what is observed in arterioles in the physiological situation. These non-dimensional parameters of interest are now defined and their values in the current experiments are discussed in relation to the corresponding physiological values.

Changing the flow rate changes the capillary number, $\mathrm{Ca} = \mu U/\sigma$, where $U =$ characteristic fluid velocity, $\sigma =$ surface tension, and $\mu =$ fluid viscosity. The capillary number indicates the ratio of viscous forces to surface tension forces, and may be thought of as a dimensionless flow rate. At each roll angle, bubble transport is studied at flow rates of 0.06, 0.08, 0.1, 0.2 and 0.3 ml/min. These correspond to capillary numbers of 1.64E-05, 2.19E-05, 2.74E-05, 5.47E-05 and 8.21E-05 respectively. The range of capillary numbers observed in arterioles in the human circulation, based on properties of blood and perfluorocarbon, is 6.51E-04–4.89E-04 (Chang et al., 1981; Halpern and Gaver, 1994; Ghadiali and Gaver, 2003; Calderon et al., 2005). The Reynolds number, $Re = UD_{\mathrm{P}}\rho/\mu$, an indicator of the relative magnitudes of inertial and viscous forces, is also a function of the flow rate. Here, D_{P} is the diameter of the parent tube while U, μ and ρ are the average velocity (in the parent tube), viscosity and density of the core fluid (water), respectively. The Reynolds numbers corresponding to the above flow rates are 1.33, 1.77, 2.21, 4.42 and 6.63. The range of Reynolds numbers observed in arterioles in the human circulation, based on properties of blood and perfluorocarbon, is 1.04–2.93E-01 (Chang et al., 1981; Halpern and Gaver, 1994; Ghadiali and Gaver, 2003; Calderon et al., 2005).

Another non-dimensional parameter of interest is the Bond number, $Bo = \Delta\rho g D_{\mathrm{P}}^2/\sigma$, where $\Delta\rho$ is the density difference between the core fluid and the bubble, g is the gravitational acceleration, D_{P} is the parent tube diameter, and σ is the surface tension between the core fluid and bubble gas (water and air in our case). The Bond number is an indicator of the relative magnitudes of forces due to gravity and surface tension. In order to include the effect of varying roll angles, a modified Bond number can be defined as $Bo^* = Bo \cdot \sin(\theta)$ (Calderon et al., 2005). Although the Bond number in these experiments is higher than the physiological value expected in arterioles, it is the modified Bond number that is of interest when considering the applicability of these results to physiological situations. Small values of the roll angle, θ, can be used to make the modified Bond numbers mimic the physiological values of Bond numbers. The Bond number in this study is $Bo = 3.58\text{E-}02$. Experiments are conducted at roll angles of 0, 15, 30 and 45°. This corresponds to modified Bond numbers, Bo^*, of 0, 9.3E-03, 1.79E-02 and 2.53E-03. The range of Bond numbers observed in arterioles in the human circulation, based on properties of blood and perfluorocarbon, is 2.0E-03—2.81E-04 (Chang et al., 1981; Halpern and Gaver, 1994; Ghadiali and Gaver, 2003; Calderon et al., 2005).

3. Results and discussion

Five runs were conducted for all combinations of roll angles and flow rates. The number of runs was selected to achieve statistical significance. All results presented here are averages over the runs corresponding to each flow condition. The error bars in all graphs indicate the standard error of the mean.

Fig. 3 presents the splitting ratio of the bubble as a function of capillary number at the four roll angles considered. Here, the splitting ratio is defined as the ratio of the volume of the bubble in the lower half of the bifurcation (V_b) after it has passed through the first bifurcation to the volume of the bubble in the upper half of the bifurcation (V_t). For $\theta = 0°$, the bubbles split nearly evenly at the first bifurcation. The evenness in splitting is clearer at the higher flow rates. In order to make sure that the machining of the bifurcation is symmetric, the bifurcation model was flipped over, and symmetric bubble splitting was again observed at roll angle equal to zero. Then data was collected for non-zero roll angles. At low flow rates even small perturbations (possible sources of perturbations/errors are discussed below) lead to instability in the splitting behavior of the bubble. This is reflected in the large error bars at the lower flow rates. This is similar to observations by Baroud et al. (Baroud et al., in press) in their investigation of a low-viscosity finger propagating through a single horizontal fluid-filled bifurcation as a model of airway reopening. In the absence of compliance elements at the ends of daughter branches of the bifurcation, uneven splitting of the finger always occurred in their model experiments. Based on linear stability analysis they concluded that any perturbation that increases the finger in one branch of the bifurcation compared to the length of the finger in the other branch leads to growth in the asymmetry due to the reduction in viscous resistance in the fluid-filled branch ahead of the longer finger. In our experiments, we observe that this instability is more pronounced as the capillary number approaches 2.74E-05. As the roll angle is increased, the splitting ratio decreases as expected. This simply indicates that a larger portion of the bubble travels to the upper half of the bifurcation due to buoyancy. The effect of gravity is more pronounced at lower flow rates. Higher flow rates increase the homogeneity in splitting.

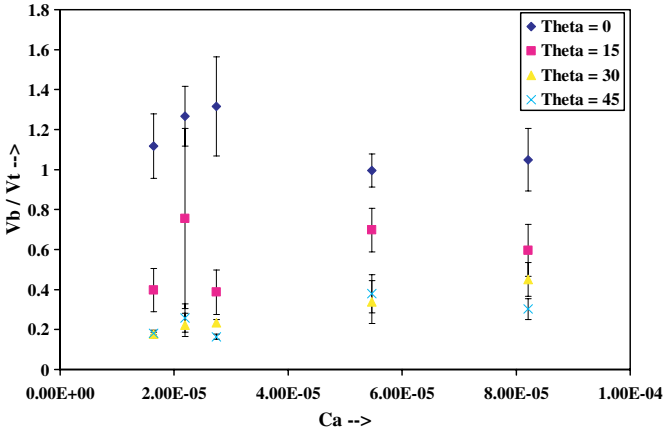

Fig. 3. Splitting ratio ($=V_b/V_t$) vs. capillary number for roll angles of 0°, 15°, 30° and 45°. At zero roll angle splitting is almost even as expected. Splitting ratio decreases with increasing roll angles. Higher flow rates lead to more homogeneous splitting.

Fig. 4 studies the bubble splitting at the lower second bifurcation in detail. The volume ratios V_1/V_0, V_3/V_0, and V_4/V_0 correspond to the ratio of bubble volume in sections L1, L3, and L4 divided by the initial bubble volume, V_0, respectively. These are referred to as V_1 ratio, V_3 ratio and V_4 ratio in this discussion. The sections L1, L3, and L4 are shown in Fig. 1. For $\theta = 0°$, the V_1 ratio is zero for higher capillary numbers, indicating that the bubble passes entirely through the bifurcation. When the capillary number is low, V_1 ratio is small and non-zero. A non-zero value of V_1 ratio indicates bubble sticking at the lower second bifurcation. V_3 ratio is consistently higher than V_4 ratio. A larger portion of the bubble enters L3 as compared to L4 as the bubble splits through the second bifurcation. It is thought that since the flow is already "turning" after passing through the first bifurcation, L3 is the more natural choice for the bubble to enter. This would explain why a larger portion of the bubble enters L3 compared to L4. As the roll angle is increased to 15° we observe non-zero values of V_1 ratio for the entire range of capillary numbers considered. Since the syringe pump is supplying a constant flow rate, once the bubble sticks at the lower second bifurcation in this manner, the entire flow is diverted into the upper half of the bifurcation. This is a significant result with respect to the gas embolotherapy application since such sticking is desirable to better occlude blood flow to the tumor. Here, we have a bubble sticking as the first generation daughter tube bifurcates into second generation daughter tubes of a smaller diameter. This corresponds to the sticking behavior discussed by Chang et al. (Chang et al., 1981). Three phase solid–liquid–gas contact lines form at the ends of the bubble, and the net surface tension contact force acting at these contact lines balances the pressure drop across the bubble. As the roll angle is further increased to 30° and 45°, we continue to observe this sticking of the bubble at the lower second bifurcation for the entire range of capillary numbers. For $\theta = 45°$ the values of V_3 ratio and V_4 ratio become comparable i.e. the bubble does not consistently prefer L3. The effect of gravity in pushing the bubble towards L4 counteracts the flow "turning" effect and the bubble does not have a strong preference for L3.

Some salient features of the flow are shown in Fig. 5, which presents a series of snapshots for a low flow rate ($Q = 0.06$ ml/min; Ca = 1.64E-05) at zero roll angle. We see that although the final state is a nearly even splitting, as would be expected when the effect of gravity is absent, the intermediate stages are not symmetrical. The bubble repeatedly sticks and slides in the different channels. This corresponds to the fact that at low capillary numbers even

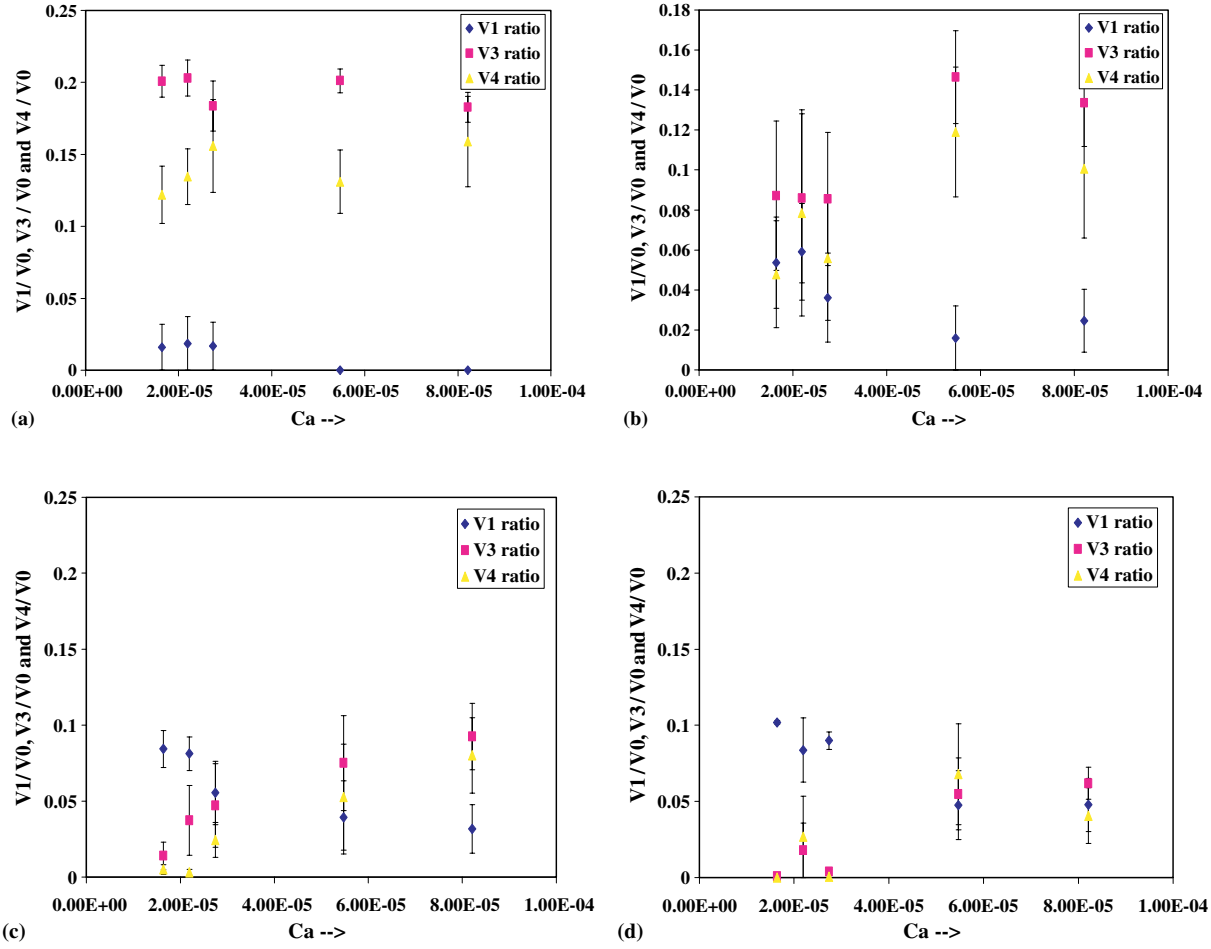

Fig. 4. Bubble volume in lower first generation branch (V_1/V_0) and subsequent lower second generation branches (V_3/V_0 and V_4/V_0) vs. Ca, for (a) $\theta = 0°$, (b) $\theta = 15°$, (c) $\theta = 30°$ and (d) $\theta = 45°$. As roll angle increases bubble sticking in the lower second bifurcation occurs for wider range of capillary numbers (this corresponds to non-zero values of V_1/V_0).

small perturbations affect the flow significantly. Contact angle hysteresis also plays an important role here. Once the bubble sticks at a certain location and a three phase solid–liquid–gas contact line forms, the contact angle must decrease below a critical value for the bubble to slide (Chang et al., 1981). While this adjustment in contact angle takes place where the bubble is stuck, the flow is diverted through the other branches of the bifurcation.

Until now we have discussed the sticking of the bubble at the lower second bifurcation. However, we also observed sticking of the bubble in the smallest second generation daughter tubes after the bubble had completely passed through both bifurcations. This is shown in Fig. 6. Here, we see a series of snapshots for $Q = 0.1$ ml/min (Ca = 2.74E-05) at a roll angle of 15°. As expected a larger portion of the bubble goes into the upper portion after splitting at the first bifurcation. At both the lower and upper second bifurcations, we observe a complete splitting of the respective bubbles. After this second splitting of the bubbles, the longest bubble (in L6) continues to move due to significant buoyancy force and exits the system. The remaining three bubbles (in L3, L4 and L5) stick in their respective second generation daughter tubes and the entire flow is diverted through L6. This indicates that sticking behavior can be expected in smaller arterioles and capillaries in the absence of strong buoyancy forces. Note that here we have sticking in a tube where the cross section does not vary. A close look reveals that both the menisci are in the same direction when the bubble sticks in this fashion. Thus, the surface tension at both the front and rear menisci opposes the flow and the bubble can stick.

Fig. 7 shows an example of a situation in which both kinds of bubble sticking are observed, i.e. sticking at a bifurcation as well as in the small diameter second generation daughter tube. Here, a series of snapshots for $Q = 0.08$ ml/min (Ca = 2.19E-05) at a roll angle of 30° are presented. As expected for a low flow rate combined with a high roll angle, gravity is very dominant and a very large portion of the bubble goes into L6. This portion of the bubble continues moving due to significant buoyancy force and exits the bifurcation model. The entire flow is then diverted through this channel. The portion of bubble that had entered L5 sticks in the tube. We also observed a sticking of the bubble in the lower part of the bifurcation

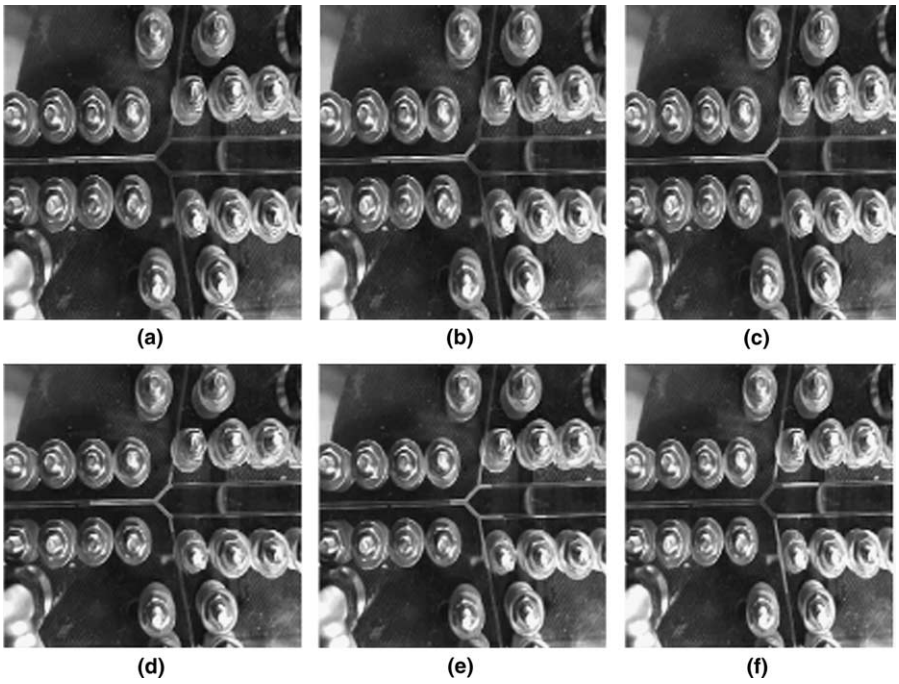

Fig. 5. Snapshots of bubble transport for $\theta = 0°$ and $Q = 0.06$ ml/min (Ca = 1.64E-05) at (a) $t = 15.0$ s, (b) $t = 17.5$ s, (c) $t = 20.0$ s, (d) $t = 22.5$ s, (e) $t = 27.5$ s. and (f) $t = 32.5$ s. Although the eventual splitting of the bubble is fairly homogeneous as expected, homogeneity is not observed at all times while the bubble is passing through the bifurcations. For small flow rates even small perturbations have a significant effect on the overall bubble dynamics.

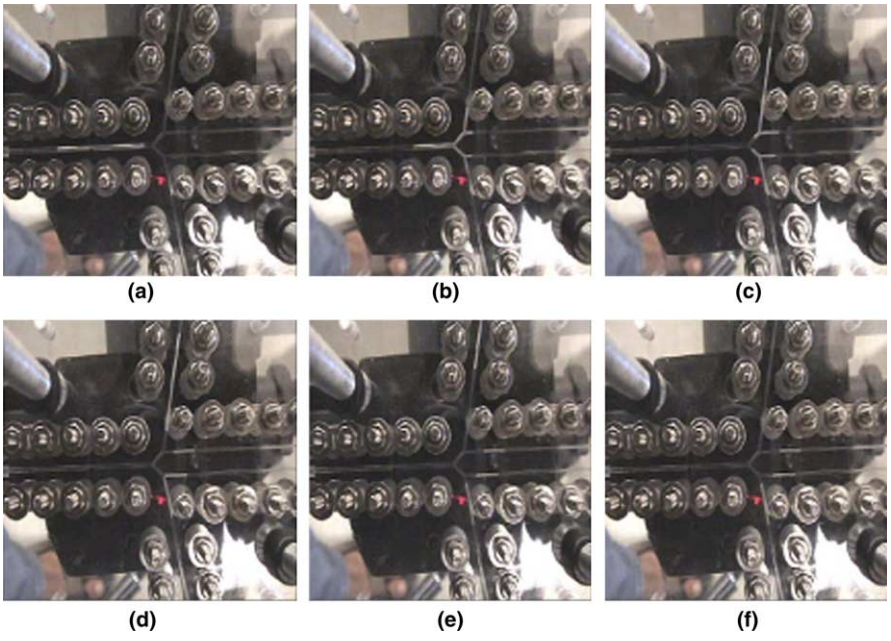

Fig. 6. Snapshots of bubble transport for $\theta = 15°$ and $Q = 0.1$ ml/min (Ca = 2.74E-05) at (a) $t = 2.5$ s, (b) $t = 7.5$ s, (c) $t = 10.0$ s, (d) $t = 11.5$ s, (e) $t = 14.0$ s. and (f) $t = 16.5$ s. The bubble in the uppermost second generation daughter tube (L6) continues to move and leaves the bifurcation model. Bubbles in the remaining second generation daughter tubes (L3, L4 and L5) stick. All the flow is diverted through L6.

model at the second lower bifurcation. An effective strategy will likely combine sticking at both locations to ensure adequate occlusion of blood flow to the tumor.

This study represents an idealization of an inherently complex physiologic flow situation, and consequently there are a number of limitations. For example, the fluidics channels do not exactly mimic arterioles, which are lined with endothelial cells and are filled with blood rather than water. Rather these experiments are intended to match relevant dimensionless parameters and provide insights into the governing fluid mechanics. This work is a first step in understanding the phenomena, and subsequent studies

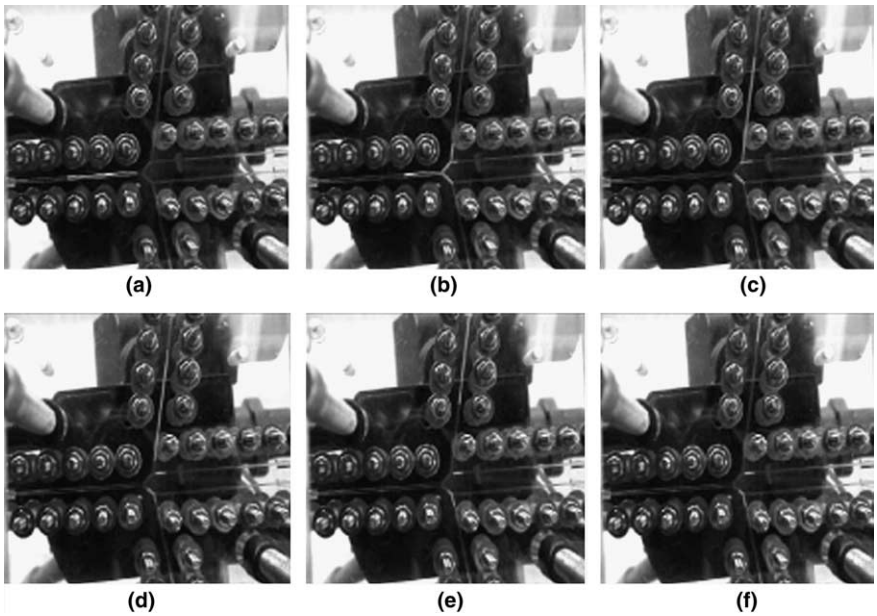

Fig. 7. Snapshots of bubble transport for $\theta = 30°$ and $Q = 0.08$ ml/min (Ca = 2.19E-05) at (a) $t = 1.5$ s, (b) $t = 6.0$ s, (c) $t = 12.0$ s, (d) $t = 14.0$ s, (e) $t = 18.0$ s and (f) $t = 22.0$ s. Both types of bubble sticking observed—in the lower second bifurcation as well as in one of the second generation daughter tubes (L5). The longest bubble in the uppermost second generation daughter tube (L6) continues to move and leaves the bifurcation model. All the flow is diverted through L6.

are needed to determine the contributions of cellular components of blood and endothelial cells (Wong and Bull, 2005). The current experiments use a constant flow rate condition, which does not allow complete occlusion of the bifurcation network. However, complete occlusion of the tumor vasculature is possible in the physiologic situation because blood flow will be shunted away from the tumor vasculature as it becomes occluded. In these bench top experiments, flow is directed to the sections of the bifurcating tube network that are not occluded, suggesting that a subsequent dose of bubbles would likely be carried to the un-occluded sections. Therefore, multiple doses may be an effective clinical strategy, and this could be explored in future studies.

Some possible sources of error in this study include small machining asymmetries, variations in the tightness of bolts along the channels, all the channels not being precisely in the same plane due to clamping of the model to the stand, small differences in the lengths of the tygon tubing (thus changing the resistance), etc. All of these appear to be quite small and efforts were made to minimize sources of error. As was pointed out in the above discussion, bubble splitting at the lower flow rates appears somewhat unstable at $\theta = 0$. That is, small perturbations in the system arising from minor imperfections or asymmetries in an individual bifurcation, may cause asymmetries in splitting to grow, and this can lead to overall asymmetric splitting. Although bubble splitting was on average nearly even for $\theta = 0$, it was not always even for an individual run at the lower Ca. This is particularly relevant to gas embolotherapy and air embolism, as actual blood vessels will rarely, if ever, be truly symmetric. Future theoretical work could assess the sensitivity of bubble splitting to minor asymmetries.

4. Conclusions

Splitting at each bifurcation is nearly even when the roll angle is zero. For non-zero roll angles, splitting is less even and bubbles can stick in one side of second bifurcation even though the flow rate in the parent tube is constant. Sticking occurs in the lower second bifurcation for $\theta > 0°$ when the flow rate (Ca) is below a critical value, which depends on θ. In addition to bubbles sticking at the second bifurcation, bubble sticking was also observed in the straight second generation channels, which corresponds to the maximum surface tension force opposing the bubble motion. The homogeneity of splitting in a bifurcating vessel network will affect how uniformly tumors can be infracted. Faster flow rates result in more even splitting. The findings of this work indicate that both gravity and flow need to be considered in developing embolization protocols. The sticking of bubbles in the bifurcation sections that receive less of the flow suggests that a treatment strategy that includes multiple doses may be effective in delivering emboli to vessels not occluded by the initial dose. Subsequent bubble doses will be carried by the flow to the unblocked vessels, where they may stick to produce a more uniform tumor infarction.

Acknowledgements

We thank Andrés J. Calderón and James H. Stephen for help with the experimental setup. This work is funded by

NIH grant EB003541, NSF grant BES-0301278, and Whitaker Foundation grant RG-03-0017.

References

Baroud, C.N., Tsikata, S., Heil, M., in press. The propagation of low-viscosity fingers into fluid-filled, branching networks. Journal of Fluid Mechanics.

Branger, A.B., Eckmann, D.M., 2002. Accelerated arteriolar gas embolism reabsorption by an exogenous surfactant. Anesthesiology 96 (4), 971–979.

Bull, J., 2003. Bubble transport in gas embolotherapy. FASEB Journal 17 (4), A144.

Bull, J.L., 2005. Cardiovascular bubble dynamics. Critical Reviews In Biomedical Engineering 33 (4), 299–346.

Calderon, A.J., Bull, J.L., 2004. Homogeneity of bubble transport through a bifurcation for gas embolotherapy. FASEB Journal 18 (4), A373.

Calderon, A.J., Fowlkes, J.B., Bull, J.L., 2005. Bubble splitting in bifurcating tubes: a model study of cardiovascular gas emboli transport. Journal of Applied Physiology 99 (2), 479–487.

Cavanagh, D.P., Eckmann, D.M., 1999. Interfacial dynamics of stationary gas bubbles in flows in inclined tubes. Journal of Fluid Mechanics 398, 225–244.

Cavanagh, D.P., Eckmann, D.M., 2002. The effects of a soluble surfactant on the interfacial dynamics of stationary bubbles in inclined tubes. Journal of Fluid Mechanics 469, 369–400.

Chang, H.K., Weber, M.E., Thomson, J., Martin, R.R., 1981. Hydrodynamic features of pulmonary air embolism: a model study. Journal of Applied Physiology: Respiratory, Environmental and Exercise Physiology 47, 539–543.

DeBisschop, K.M., Miksis, M.J., Eckmann, D.M., 2002. Bubble rising in an inclined channel. Physics of Fluids 14 (1), 93–106.

Di Segni, R., Young, A.T., Zhong, Q., Castaneda-Zuniga, W.R., 1997. Embolotherapy: agents, equipment, and techniques. In: Castaneda-Zuniga, W.R. (Ed.), Interventional Radiology. Williams and Wilkins, Baltimore, pp. 81–84.

Eckmann, D.M., Cavanagh, D.P., 2003. Bubble detachment by diffusion-controlled surfactant adsorption. Colloids and Surfaces A—Physicochemical and Engineering Aspects 227 (1–3), 21–33.

Eckmann, D.M., Diamond, S.L., 2004. Surfactants attenuate gas embolism-induced thrombin production. Anesthesiology 100 (1), 77–84.

Eckmann, D.M., Cavanagh, D.P., Branger, A.B., 2001. Wetting characteristics of aqueous surfactant-laden drops. Journal of Colloid and Interface Science 242 (2), 386–394.

Fung, Y.C., 1997. Biomechanics: Circulation. Springer, New York, 571 pp.

Ghadiali, S.N., Gaver, D.P., 2003. The influence of non-equilibrium surfactant dynamics on the flow of a semi-infinite bubble in a rigid cylindrical capillary tube. Journal of Fluid Mechanics 478, 165–196.

Halpern, D., Gaver, D.P., 1994. Boundary element analysis of the time-dependent motion of a semi-infinite bubble in a channel. Journal of Computational Physics 115 (2), 366–375.

Kripfgans, O.D., Fowlkes, J.B., Miller, D.L., Eldevik, O.P., Carson, P.L., 2000. Acoustic droplet vaporization for therapeutic and diagnostic applications. Ultrasound in Medicine & Biology 26 (7), 1177–1189.

Kripfgans, O.D., Fowlkes, J.B., Woydt, M., Eldevik, O.P., Carson, P.L., 2002. In vivo droplet vaporization for occlusion therapy and phase aberration correction. IEEE Transactions on Ultrasonics Ferroelectrics and Frequency Control 49 (6), 726–738.

Kripfgans, O.D., Fabiilli, M.L., Carson, P.L., Fowlkes, J.B., 2004. On the acoustic vaporization of micrometer-sized droplets. Journal of the Acoustical Society of America 116 (1), 272–281.

Manga, M., 1996. Dynamics of drops in branched tubes. Journal of Fluid Mechanics 315, 105–117.

Suzuki, A., Eckmann, D.M., 2003. Embolism bubble adhesion force in excised perfused microvessels. Anesthesiology 99 (2), 400–408.

Suzuki, A., Armstead, S.C., Eckmann, D.M., 2004. Surfactant reduction in embolism bubble adhesion and endothelial damage. Anesthesiology 101 (1), 97–103.

Wong, Z.Z., Bull, J.L., 2005. An endothelialized, microfluidic model of a microvessel for in vitro research in gas embolotherapy. FASEB Journal 19 (4), A728-A.

Ye, T., Bull, J.L., 2004a. Computational simulation of micro-bubble expansion in gas embolotherapy. FASEB Journal 18 (4), A373.

Ye, T., Bull, J.L., 2004b. Direct Numerical Simulations of Micro-Bubble Expansion in Gas Embolotherapy. Journal of Biomechanical Engineering 126 (6), 745–759.